SUPPLEMENTARY INFORMATION

Born to Sense: Biophysical Analyses of the Oxygen Sensing Prolyl Hydroxylase from the Simplest Animal *Trichoplax adhaerens*

1. Experimental Procedures
2. Supplementary figures
3. Supplementary tables

1. Experimental Procedures

Materials

All chemicals were from Sigma Aldrich or Merck Chemicals, unless otherwise stated. Primers were from Sigma Aldrich. *Ta*ODD and *Hs*HIF1a CODD/NODD peptides, all prepared with a *C*-terminal amide, were from GL Biochem (Shanghai, China) and Chinapeptides (Suzhou, China).

Protein production, crystallisation, and structure solution

Recombinant protein production and purification

DNA sequences encoding for *N*-terminally truncated and His_6-tagged *Ta*PHD$^{64-300}$ and *Hs*PHD2$^{181-426}$ in the pET28a(+) vectors were expressed and the resultant proteins were purified as described in [1] and [2]. *Hs*PHD2$^{181-426}$ variants were produced as described.[3] All constructs were verified by DNA sequencing.

Vectors encoding for *Ta*PHD$^{64-300}$ and *Hs*PHD2$^{181-426}$ were transformed into *E. coli* BL21(DE3) cells. Recombinant protein production was induced with 0.5 mM isopropyl-β-D-thiogalactosidase (*Ta*PHD$^{64-300}$: 4 h at 28 °C, followed by overnight growth at 18 °C, *Hs*PHD2$^{181-426}$: 4 h at 28 °C). Cells were harvested and lysed by sonication in Tris-HCl (20 mM, pH 7.5) and NaCl (0.5 M); (glycerol (5 %) and DTT (5 mM) were added in the case of the *Ta*PHD$^{64-300}$ and *Hs*PHD2$^{181-426}$ variants). Proteins were purified by Ni^{2+} affinity chromatography followed by size exclusion chromatography as reported.[1] Proteins were of > 95% purity, as determined by SDS-PAGE, and characterised by liquid chromatography-mass spectrometry analysis (Figure S8).

The S177R and P213R *Ta*PHD variants were prepared using DNA encoding for *N*-terminal truncated and His_6-tagged wild-type *Ta*PHD$^{64-300}$ in the pET28a(+) vector by site-directed mutagenesis. Expression and purification were carried out as described for the wild-type *Ta*PHD$^{64-300}$.[1] The vector encoding for the required proteins was transformed into *E. coli* BL21(DE3) and protein production was induced with 0.5 mM isopropyl-β-D-thiogalactosidase (4 h at 28°C, then overnight at 18°C). Cells were harvested and lysed by sonication in Tris-HCl (20 mM), pH 7.5, and

NaCl (0.5 M). The proteins were purified by Ni^{2+} affinity chromatography followed by size exclusion chromatography.[1]

Crystallisation

Crystallisation screens were carried out using the sitting drop vapour diffusion method in low profile 96 well/3-subwell Art Robbins Intelliplates (Hampton Research, CA, USA) and an Art Robbins PHENIX-RE automated liquid dispenser was used with 200-300 nL total drop volumes (1:2, 1:1, and 2:1 protein:well solution ratios) with 80 µL of precipitant solution in the well. Wells were sealed with StarSeal Advanced Polyolefin Film (STARLAB, UK). *Ta*PHD protein was used at 20 mg/mL in Tris-HCl (50 mM, pH7.5). Irregular crystals of *Ta*PHD with $Mn(II)Cl_2$ (2 mM) and IOX3 (2 mM, [4]) were obtained at 4 °C in conditions containing ammonium acetate (0.2 M), polyethylene glycol 3350 (25 % $^{w}/_{v}$), bis-tris (0.1 M, pH 5.5), and *Ta*PHD protein. Initial crystallisation conditions were optimised at room temperature by streak seeding under identical conditions except for the absence of IOX3. Crystals of the *Ta*PHD.*Ta*ODD complex with $Mn(II)Cl_2$ (1 mM) and NOG (2 mM) were obtained at 20 °C in a buffer condition containing ammonium acetate (0.31 M), polyethylene glycol 3350 (24 % $^{w}/_{v}$), bis-tris (0.1 M, pH 5.5), and 21mer *Ta*HIFα ODD peptide (*Ta*HIFα$^{477\text{-}497}$ EKEDYDDLA**P**FVPPPSFDNRL-NH_2, 10 mM). Crystals were then harvested in nylon loops (Hampton Research) by transferring into a cryo-solution containing 25 % (v/v) glycerol in the well solution, then cryo-cooled by plunging in liquid nitrogen, and were stored under liquid nitrogen until data collection.

Data Collection and Structure Solution

Data sets for the *Ta*PHD (to 1.2 Å resolution) and *Ta*PHD.*Ta*ODD (to 1.3 Å resolution) crystals were collected from single crystals at 100 K at the Diamond Light Source beamlines I04 and I02, repectively, both equipped with an ADSC Quantum 315r detector. Data were indexed, integrated and scaled using HKL-2000[5] (see Table 1 for data statistics). The *Ta*PHD crystals were space group $P2_1$ with one molecule in the asymmetric unit. The structure of *Ta*PHD was solved by molecular replacement using PHASER[6] using a structure of *Hs*PHD2 (PDB: 2G19) as the search model. The *Ta*PHD.*Ta*ODD crystals were space group *P*1 with one molecule in the asymmetric unit. The

structure of *Ta*PHD.*Ta*ODD was solved by molecular replacement using PHASER[6] and the *Ta*PHD structure as a search model. Maximum likelihood refinement including anisotropic displacement parameters for all atoms was carried out iteratively using PHENIX refine[7] and model building with COOT[8] until converging R and R_{free} values no longer decreased.

Enzymatic assays

2OG turnover monitoring by ^{1}H CPMG NMR experiments

2OG to succinate turnover was monitored by ^{1}H Carr-Purcell-Meiboom-Gill (CPMG) NMR experiments; typical experimental parameters for CPMG NMR spectroscopy were as follows: total echo time, 40 ms; acquisition time, 2.72 s; relaxation delay, 2 s; number of transients, 64. The PROJECT-CPMG sequence (90°x−[τ−180°y−τ−90°y−τ−180°y−τ]*n*−acq) was applied.[9] Water suppression was achieved by pre-saturation. Data were processed using Bruker 3.1 software with a line broadening of 0.3 Hz. Assay mixtures contained *Ta*PHD or *Hs*PHD2 (20 μM), $(NH_4)_2Fe(II)(SO_4)_2$ (125 μM), sodium (+)L-ascorbate (1 mM), *Hs*HIF1α CODD 19mer (DLDLEMLA**P**YIPMDDDFQL-NH_2, 500 μM) or *Ta*HIFa ODD 25mer substrate (PINEKEDYDDLA**P**FVPPPSFDNRLY-NH_2, 500 μM) where necessary, 2-oxoglutarate disodium salt (400 μM), in 10 % D_2O and 90 % H_2O, Tris-D_{11} (50 mM), pH 7.5.

*^{13}C- HsHIF*1α *CODD and ^{13}C- HsHIF*1α *NODD displacement experiments*

The 1D CLIP HSQC displacement experiments were conducted using a Bruker AV700 instrument. 3 mm MATCH NMR tubes were used (Cortecnet). All experiments were performed at 298 K. The reporter *Hs*HIF1α CODD/NODD peptide (DLDLEMLA**P**YIPMDDDFQL-NH_2/DALTLLA**P**AAGDTIISLDF-NH_2) was ^{13}C labelled on all carbons in its proline ring. The CLIP-HSQC sequence was used for 1D HSQC experiments (without ^{13}C decoupling). A relaxation delay of 2 s was applied. The $^{1}J_{CH}$ was set to 160 Hz. A 6.8 ms Q3.1000 180 degree pulse was used and selective irradiation was applied at the selective chemical shift. Assay mixtures contained ^{13}C-proline *Hs*HIF1α CODD/NODD (50 μM), *Ta*PHD (50 μM) (where necessary), 2-oxoglutarate disodium salt (50 μM) buffered with Tris-D_{11} (50 mM), pH 7.5, in 10 % D_2O and 90 % H_2O.

MALDI–TOF-MS enzymatic assays

Matrix-assisted laser desorption/ionization time-of-flight mass spectrometry (MALDI-TOF-MS) assays were performed using a Waters® Micromass® MALDI micro MX™ mass spectrometer using a modified version of the reported procedure.[10] Unless otherwise stated, the following conditions were used: *Hs*PHD2 or *Ta*PHD (3.5 μM), *Hs*HIF1α CODD (DLDLEMLA**P**YIPMDDDFQL-NH_2, 100 μM) or *Ta*HIFα ODD substrate (PINEKEDYDDLA**P**FVPPPSFDNRLY-NH_2, 100 μM), $(NH_4)_2Fe(II)(SO_4)_2$ (50 μM), sodium L-ascorbate (4 mM) and 2-oxoglutarate disodium salt (300 μM) in Tris (50 mM), pH 7.5. The reactions were incubated at 25 °C and quenched with formic acid (1 % $^{v}/_{v}$) at various time points. For steady-state kinetic experiments, the initial rates were determined by varying the concentration of one of the substrates/co-substrates (*Hs*HIF1α CODD, *Ta*ODD or 2OG) and maintaining fixed saturating concentrations of the other component. Hydroxylation levels were quantified using MassLynx™ V4.0. K_m and k_{cat} values were determined using GraphPad Prism®.

The O_2-dependence of the reaction was determined according to the reported procedure[11] with a *Ta*PHD concentration of 4 μM. For safety reasons, it was not possible to test O_2-concentrations > 60 %.

2. Supplementary figures

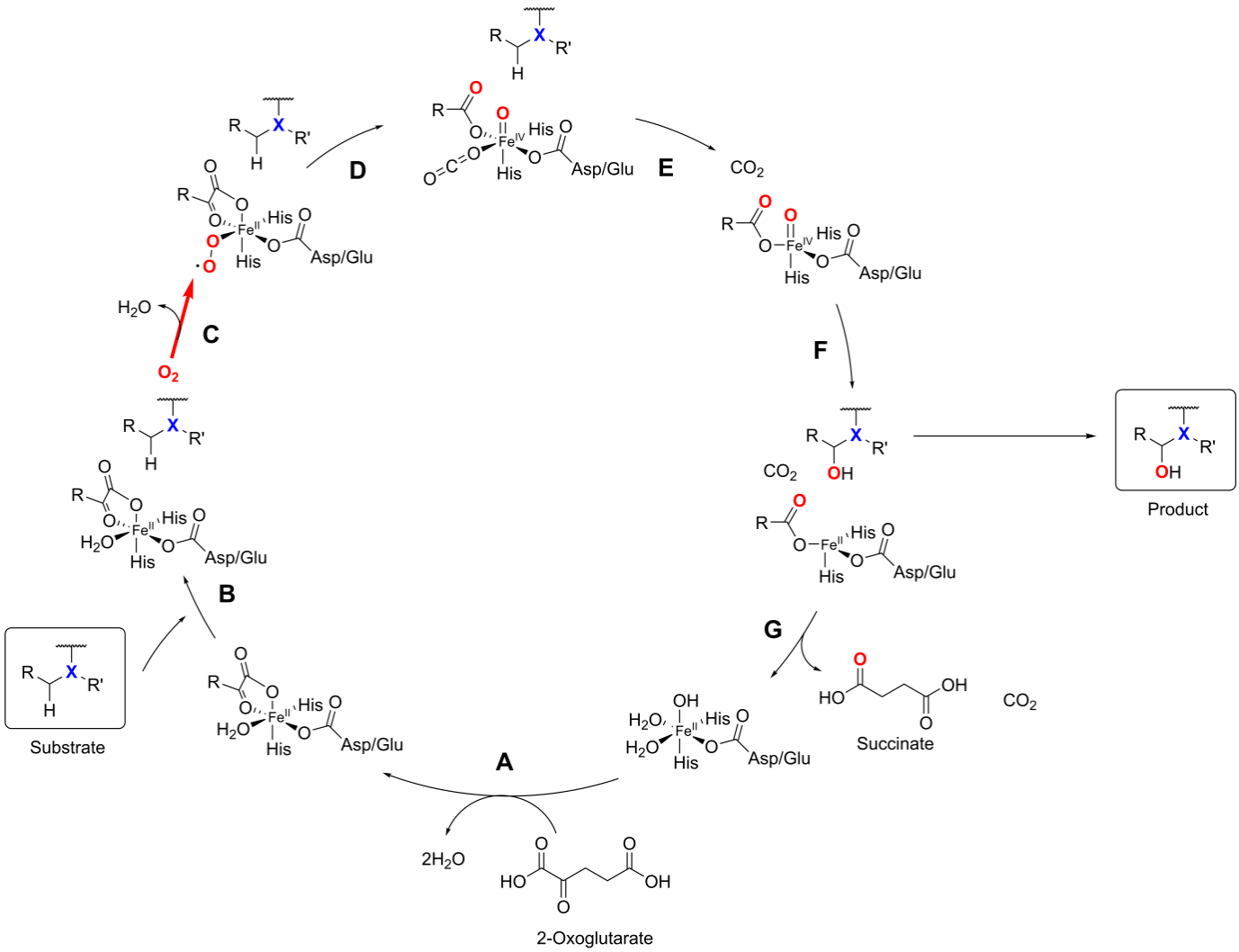

Figure S1 | Outline of the consensus 2OG oxygenase mechanism. Within the active site, Fe(II) is initially bound in a 6-coordinate manner by a conserved HX(D/E)...H motif and 2-3 water molecules, 2 of which are displaced on binding of 2-oxoglutarate (2OG, **A**). Subsequent binding of the substrate (**B**) then oxygen (**C**) leads to the displacement of the third water molecule. Binding of oxygen to the active site Fe(II) in *Hs*PHD2 has been proposed to be the rate limiting step in prolyl-hydroxylation.[12] Oxidative decarboxylation of 2OG generates CO_2 and succinate, leading to formation of a reactive Fe(IV)=O intermediate, which enables hydroxylation of the substrate (**D**-**G**).

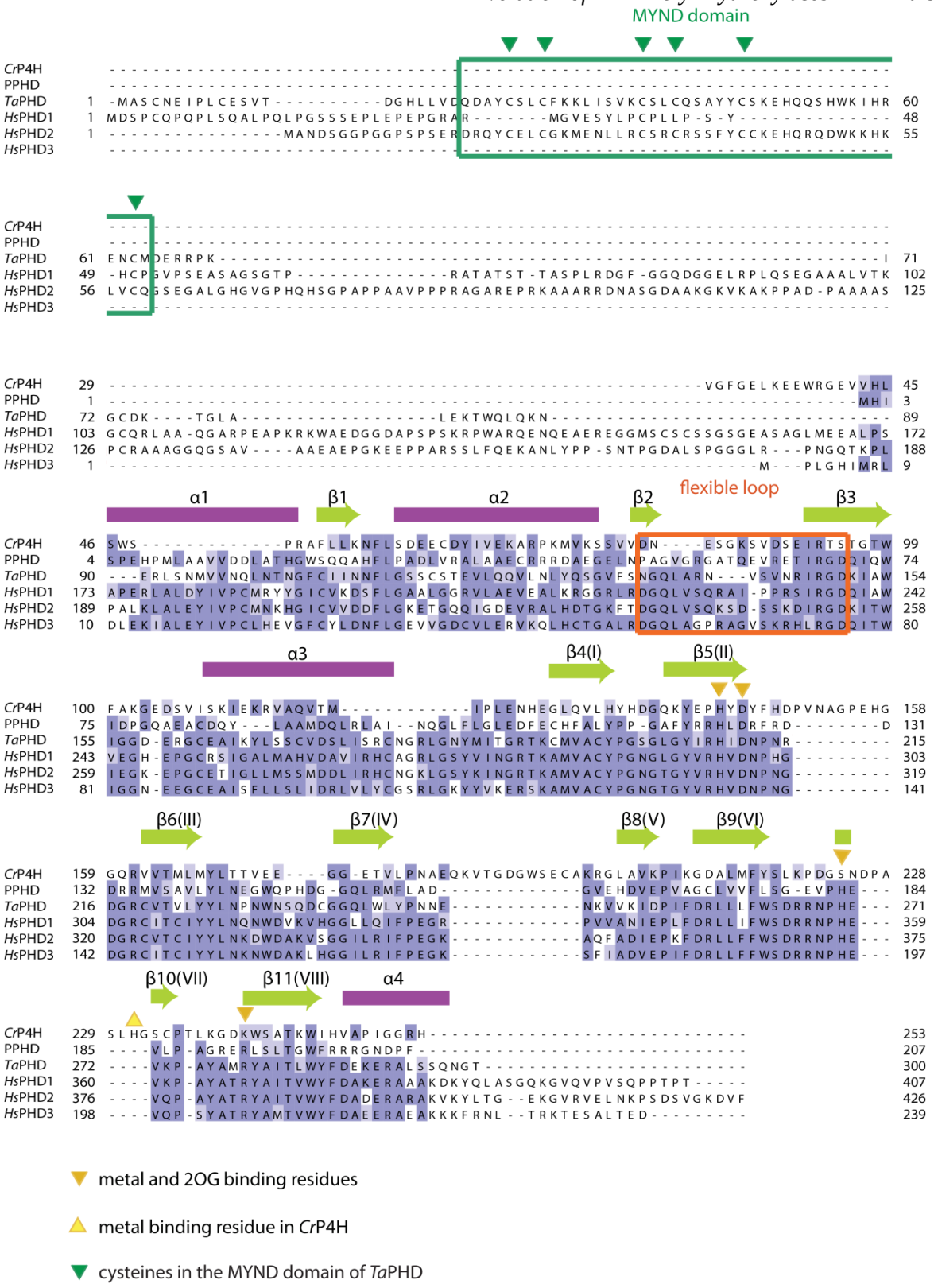

Figure S2 | Comparison of the sequences of human PHD isoforms 1-3 with those for *Ta*PHD, *Cr*P4H and *Pseudomonas Putida* PPHD. Sequences corresponding to the myeloid, Nervy, and DEAF-1 (MYND) motif and the flexible β2/β3-finger-loop are boxed, α-helices are marked purple, and β-sheets are labelled with green arrows. The alignment was generated using Clustal Omega[13] and Jalview 2.9.0b2.[14]

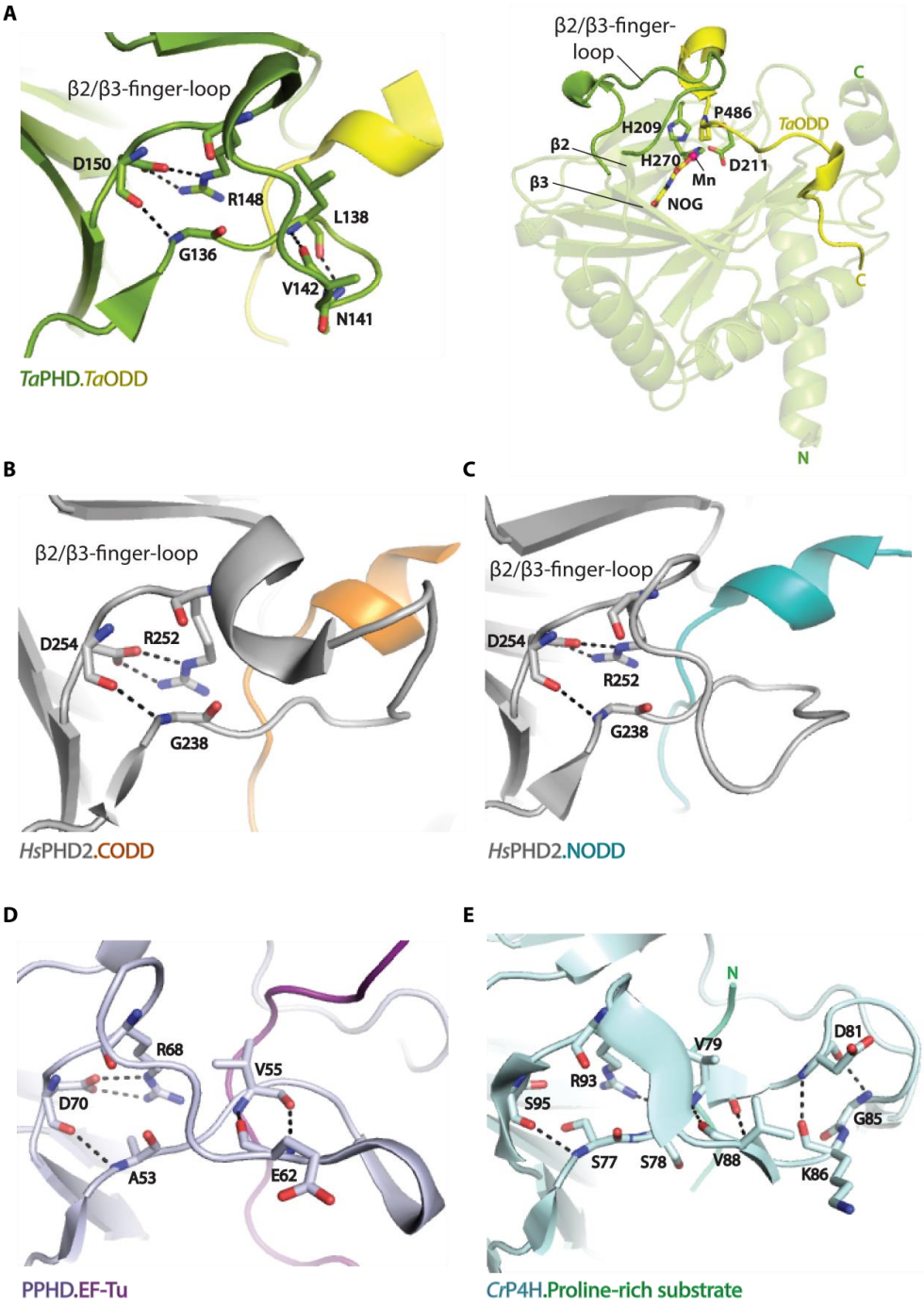

Figure S3 | Views of the β2/β3-finger-loop in the (A) *Ta*PHD.*Ta*ODD, (B) *Hs*PHD2.CODD (PDB: 3HQR, [2]), (C) *Hs*PHD2.NODD (PDB: 5L9V, [3]), (D) PPHD.EF-Tu, (PDB: 4IW3, [15]), and (E) *Cr*P4H.Proline-rich substrate (PDB: 3GZE, [16]) structures. Hydrogen bonding and electrostatic interactions between loop-residues are displayed. Notably, the β2/β3-finger-loop in the *Ta*PHD.*Ta*ODD structure adopts a condensed, finger-like shape, which is stabilised via intra-loop-interactions.

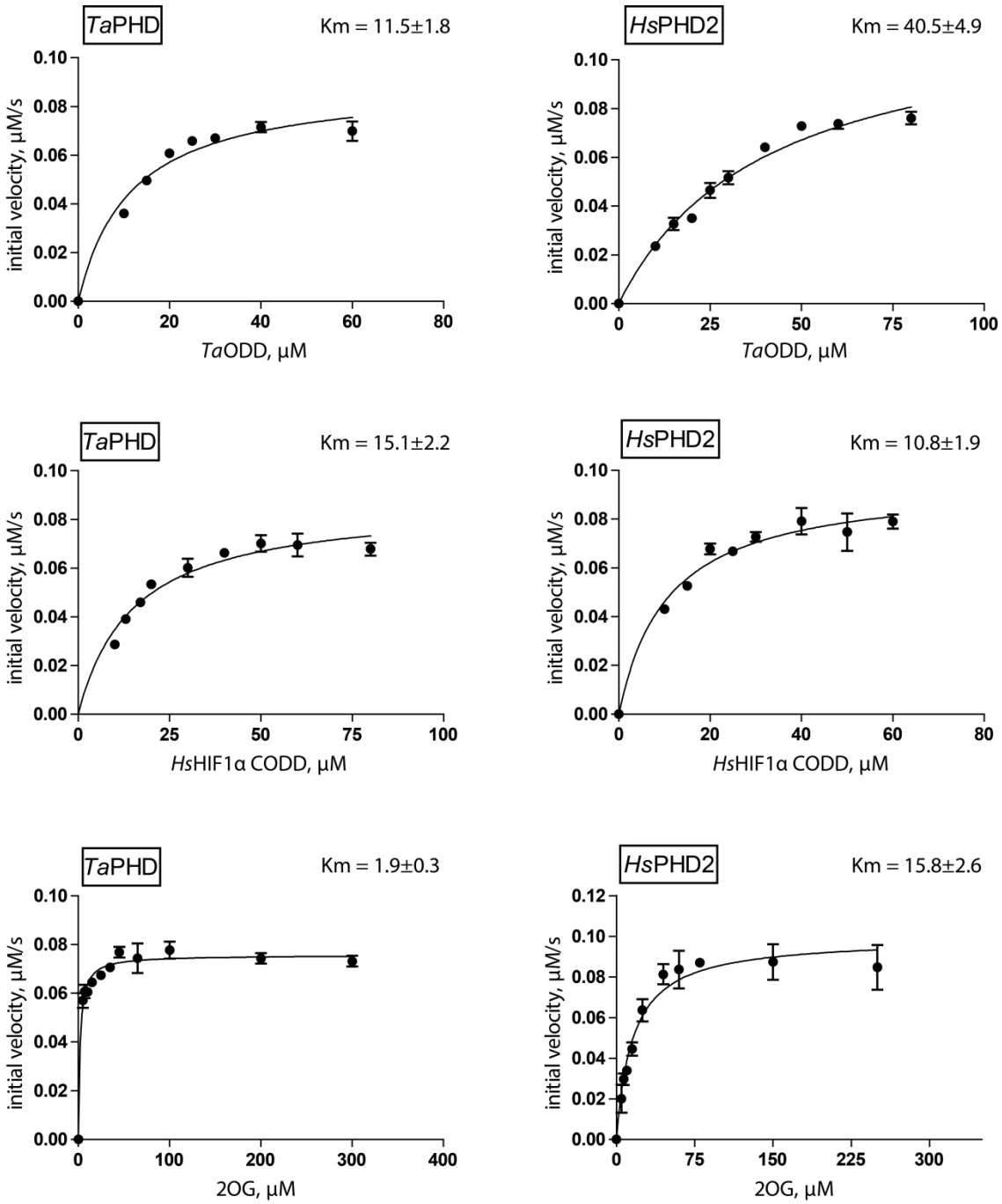

Figure S4 | Comparison of kinetic parameters for *Ta*PHD and *Hs*PHD2. Conditions: *Hs*PHD2 or *Ta*PHD (3.5 µM-7.0 µM), *Hs*HIF1α CODD 19mer peptide (DLDLEMLA**P**YIPMDDDFQL-NH_2, 100 µM) or *Ta*HIFα ODD 25mer peptide (PINEKEDYDDLA**P**FVPPPSFDNRLY-NH_2, 100 µM), $(NH_4)_2Fe(II)(SO_4)_2$ (50 µM), sodium L-ascorbate (4 mM) and 2-oxoglutarate disodium salt (300 µM) in Tris (50 mM), pH 7.5.[10] Initial rates were determined by varying the concentration of the respective peptide or 2OG. Peptide hydroxylation was analysed by MALDI-MS, 'background' (i.e. non-enzymatic) methionine oxidation was subtracted, and the data were fitted with the Michaelis-Menten equation using GraphPad Prism® (errors are indicated as standard deviations, n=3).

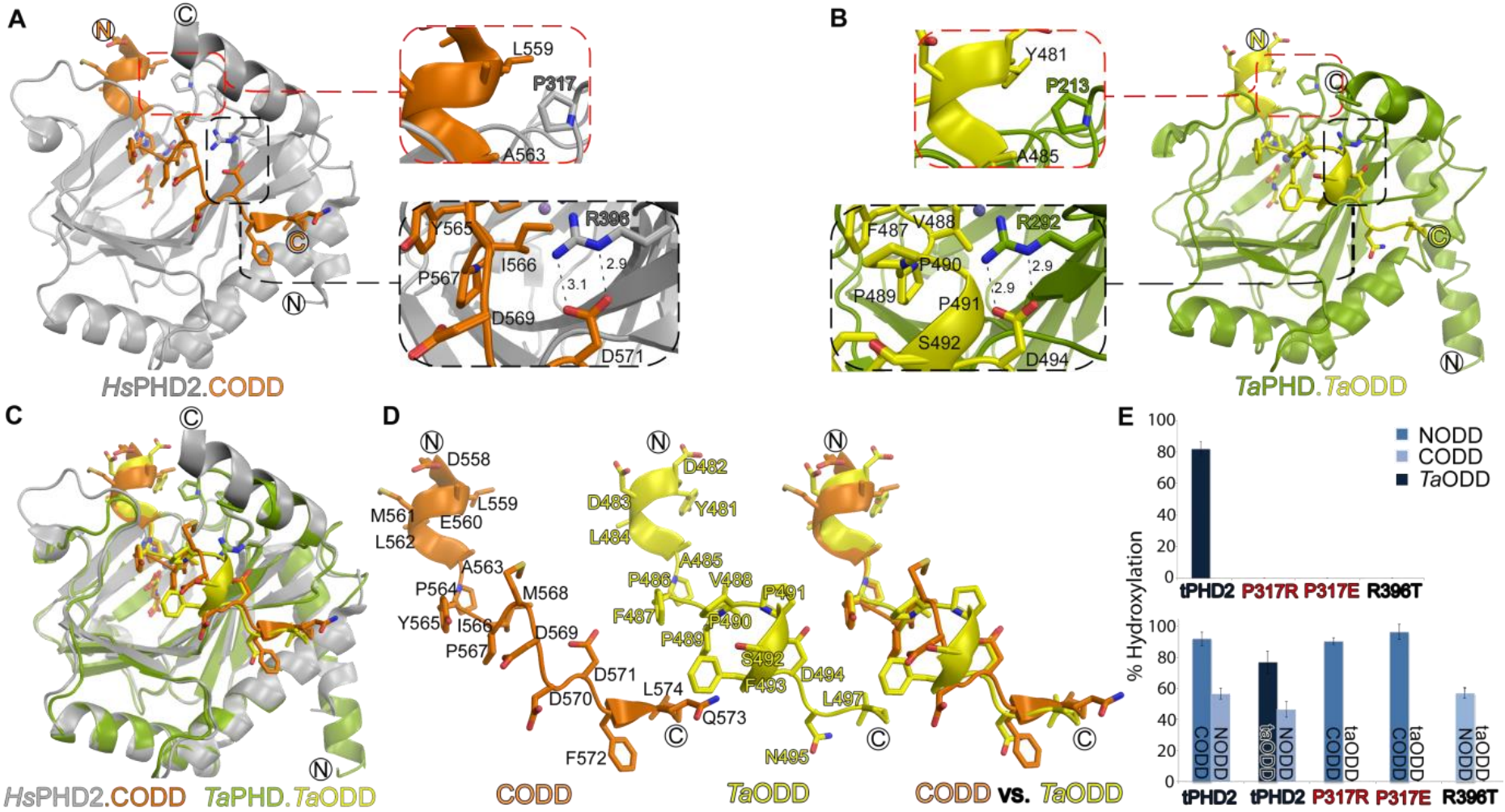
A
L559
P317
A563
Y565
R396
I566
P567
2.9
3.1
D569
D571
HsPHD2.CODD
B
Y481
P213
A485
F487
V488
R292
P490
P489
2.9
P491
S492
D494
TaPHD.TaODD
C
HsPHD2.CODD
TaPHD.TaODD
D
D558
L559
M561
E560
L562
A563
P564
M568
Y565
I566
D569
P567
D571
D570
L574
Q573
F572
CODD
D482
D483
Y481
L484
A485
P486
V488
P491
F487
P490
P489
S492
F493
D494
L497
N495
TaODD
CODD vs. TaODD
E
% Hydroxylation
NODD
CODD
TaODD
tPHD2
P317R
P317E
R396T

Figure S5 | Analyses of *Hs*PHD2 and *Ta*PHD substrate complexes and assay results indicate a conserved mode of ODD binding to both *Hs*PHD2 and *Ta*PHD. (A-C) Comparison of *Hs*PHD2.CODD (PDB: 3HQR, [2]), *Hs*PHD2.NODD (PDB: 5L9V, [3]), and *Ta*PHD substrate structures reveals similar binding modes for *Ta*ODD and *Hs*HIF1α CODD. These include a salt-bridge between $R292_{TaPHD}$ and $D494_{TaODD}$ (analogous to the salt-bridge between $R396_{HsPHD2}$ and $D571_{HsHIF1\alpha\ CODD}$) and hydrophobic interactions with $P213_{TaPHD}$ (analogously positioned $P317_{HsPHD2}$) and the YXXLAP/ LXXLAP motif. **(D)** Comparison of *Hs*HIF1α CODD and *Ta*ODD conformations as observed in the *Hs*PHD2.CODD and *Ta*PHD.*Ta*ODD complexes.[10] **(E)** Endpoint hydroxylation assays with *N*-terminally truncated wild-type *Hs*PHD2 (tPHD2), and the $R396_{HsPHD2}$ and $P317_{HsPHD2}$ variants; (errors are indicated as standard deviations, n=3). Heterozygous mutations to $R396_{HsPHD2}$ and $P317_{HsPHD2}$ have been observed in patients with cancer and erythrocytosis.[17-19] The $R396T_{HsPHD2}$ variant is highly selective for NODD over CODD, as it is not able to form the salt-bridge with CODD ($R396_{HsPHD2}$ - $D571_{HsHIF1\alpha\ CODD}$). The $P317R_{HsPHD2}$ variant is selective for CODD, as it forms less hydrophobic interactions (with both ODDs) than the wild-type *Hs*PHD2. However, because hydrophobic interactions with the LXXLAP residues play relatively more important roles in NODD compared to CODD catalysis,[3] $P317R_{HsPHD2}$ does not hydroxylate *Hs*HIF1α NODD.[3] The $P317_{HsPHD2}$ and $R396_{HsPHD2}$ residues, which are conserved in almost all PHDs in metazoans, were used to test if *Hs*PHD2 binds *Ta*ODD similarly as *Hs*HIF1α CODD and NODD. The endpoint assay results (**E,** top**)** show that while tPHD2 can hydroxylate *Ta*ODD, both $P317R_{HsPHD2}$ (and $P317E_{HsPHD2}$) and $R396T_{HsPHD2}$ variants were inactive on *Ta*ODD (within detection limits), in a similar manner as the indicated tPHD2 variants lose their ability to hydroxylate *Hs*HIF1α NODD or *Hs*HIF1α CODD (respectively). Thus, the results of the assays in the upper panel support similar binding modes for *Ta*ODD and *Hs*HIF1α CODD/NODD to *Hs*PHD2. Competition experiments were carried out (lower panel), where equimolar amounts of two ODDs (in a single assay mixture) were incubated with tPHD2, and the *Hs*PHD2 variants $R396_{HsPHD2}$ and $P317_{HsPHD2}$ **(E,** bottom**)**. The results imply that *Hs*PHD2 accepts the different ODDs with an order of activity of *Hs*HIF1α CODD > *Ta*ODD > *Hs*HIF1α NODD.

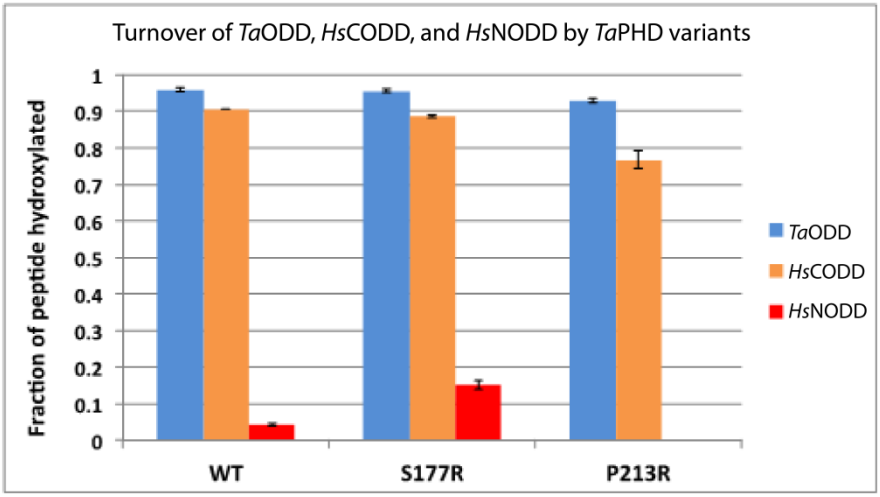

Figure S6 | Effect of S177R$_{TaPHD}$ and P213R$_{TaPHD}$ substitutions on catalysis by *Ta*PHD. The activity of the *Ta*PHD variants was measured using end-point hydroxylation assays (3 h incubation, 25 °C) (errors are indicated as standard deviations, n=3). Conditions: *Ta*PHD (3.5 μM), *Ta*HIFα ODD/*Hs*CODD/*Hs*NODD(100 μM), $(NH_4)_2Fe(II)(SO_4)_2$ (50 μM), sodium L-ascorbate (4 mM) and 2-oxoglutarate disodium salt (300 μM) in Tris (50 mM), pH 7.5.[10] The residue R281$_{HsPHD2}$ that interacts with D412 within the NODD of *Hs*HIF1α,[3,20] is conserved in *Hs*PHD1 (R265), but not in *Ta*PHD (S177) or in *Hs*PHD3 (L103) (Figure S2, Table S1); *Hs*PHD3 has a strong preference for CODD over NODD.[21,22] The S177R$_{TaPHD}$ variant manifests increased *Hs*HIF1α NODD 19mer turnover, relative to wildtype *Ta*PHD (from 4 % to 15 %), while the fraction of hydroxylated *Hs*HIF1α CODD 19mer and *Ta*ODD 25mer was not affected in the same timeframe. The clinically observed variant P317R$_{HsPHD2}$ is associated with familial erythrocytosis.[18,19] The *Hs*PHD2 variant P317R$_{HsPHD2}$ retains full activity on *Hs*HIF1α CODD, but does not (within detection limits) hydroxylate *Hs*HIF1α NODD.[3] In agreement with this, the *Ta*PHD 'analogue' P213R$_{TaPHD}$ of the clinically observed mutation did not manifest any evidence for *Hs*HIF1α NODD 19mer hydroxylation.

A

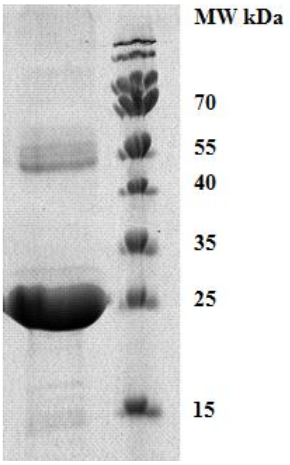

B

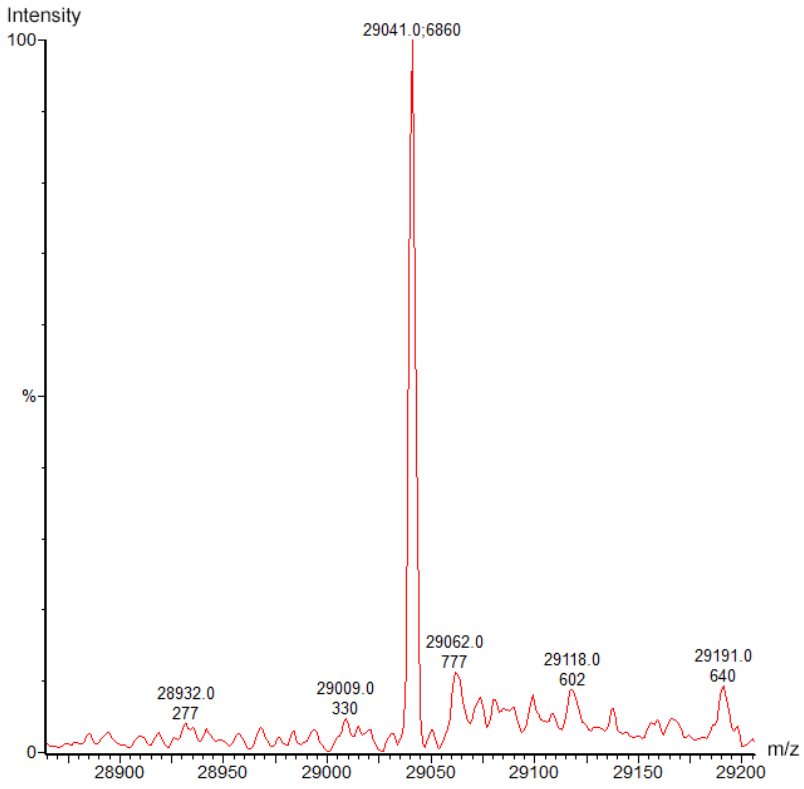

Figure S7 | Purification of *Ta*PHD$^{64\text{-}300}$. (A) SDS-PAGE gel of purified *Ta*PHD$^{64\text{-}300}$ (MW= 29.2 kDa). **(B)** Electrospray ionisation (positive ion mode)-liquid chromatography-mass spectrometry (ESI-LC-MS) spectrum of *Ta*PHD$^{64\text{-}300}$. A peak corresponding to the calculated mass of *Ta*PHD$^{64\text{-}300}$ minus the *N*-terminal methionine residue (MW = 29042 Da) is observed.

3. Supplementary tables

Table S1 | Hydrogen bonds and hydrophobic interactions between *Ta*PHD and *Ta*ODD, as observed in the *Ta*PHD.*Ta*ODD structure, compared to the *Hs*PHD2.CODD structure (PDB: 3HQR, [2]) and *Hs*PHD2.NODD (PDB: 5L9V, [3]) structures (apparent potential hydrophobic interactions were defined using a cut-off distance of 4 Å).

*Ta*PHD.*Ta*ODD		*Hs*PHD2.CODD		*Hs*PHD2.NODD		Structural region in *Ta*PHD/ *Hs*PHD2
Protein	Substrate	Protein	Substrate	Protein	Substrate	
Gln137	Phe487*†	Gln239	Tyr565*†	Gln239	Ala403*†	β2/β3
		Leu240	Tyr565*	Leu240	Pro402*	β2/β3
Ala139	Ala485*† Phe487*	Val241	Ala563*†	Val241	Thr398* Ala401*† Pro402*	β2/β3
		Ser242	Glu560*†	Ser242	Thr398*† Leu399*	β2/β3
		Lys244	Met561*	Lys244	Leu399*	β2/β3
Asn141	Phe487*					β2/β3
Ile147	Leu484*	Ile251	Leu562*	Ile251	Leu400*	β2/β3
H2O-Arg148NH	Phe487†	H2O-Arg252NH	Tyr565†	H2O-Arg252NH	Ala403†	β2/β3
Trp154	Phe487* Pro489*	Trp258	Ile566* Pro567*			β3
Asp173	Leu497*			Asp277	Leu411*	α3
		Ile280	Leu574*			α3
		Arg281	Leu574†	Cys281^{mutated}	Cys412^{X}	α3
Ile188	Leu497*	Ile292	Leu574*			α3/β4
Thr189	Leu497*†	Asn293	Leu574*†	Asn293	Leu411*†	α3/β4
Gly190	Leu497*	Gly294	Leu574*	Gly294	Ile408* Leu411*	α3/β4
Arg191	Asn495*† Leu497*	Arg295	Phe572† Leu574*	Arg295	Ile409*†	α3/β4
Thr192	Val488*					α3/β4
Lys193	Phe493*	Lys297	Asp570*	Lys297	Thr407* Ile409*	α3/β4
Tyr206	Leu484*† Pro486*†	Tyr310	Leu562† Pro564†	Tyr310	Leu400* †	β5

					Pro402*	
Ile207	Leu484*	Val311	Leu562*	Val311	Leu400*	β5
Arg208	Tyr481*†					β5
His209	Tyr481* Leu484* Pro486*	His313	Leu562* Pro564*	His313	Leu400* Pro402*	β5
Ile210	Tyr481*	Val314	Leu559*			β5
Asp211	Pro486*	Asp315	Pro564*	Asp315	Pro402*	β5
Pro213	Tyr481* Ala485*	Pro317	Leu559* Ala563*	Cys317^{mutated}	Cys397 ^{X}	β5/β6
Asp216	Val488*					β5/β6
Arg218	Pro486† Val488*	Arg322	Pro564† Ile566*	Arg322	Pro402† Ala404*	β5/β6
Arg266	Asp482†	Arg370	Leu559*	Arg370	Asp395†	β9/β10
Trp285	Pro486*	Trp389	Pro564* Ile566*	Trp389	Pro402*	β11
Tyr286	Leu497*	Tyr390	Leu574*	Tyr390	Leu411*	β11
Phe287	Val488* Asp494*	Phe391	Ile566*	Phe391	Ile408*	β11/α4
Arg292	Pro489† Asp494†	Arg396	Pro567† Met568† Asp571†	Arg396	Ile408*	α4
Ser295	Pro491*					α4
Ser296	Pro491*	Lys400	Asp571†			α4
		Tyr403	Met568*			
		Leu404	Met568*			

* Apparent potential hydrophobic interaction.

† Hydrogen bond.

^{X} Disulfide bond.

Table S2 | Analysis of structural conservation between *Ta*PHD, *Hs*PHD2, PPHD, and *Cr*P4H. Pairs of structures (structures 1 and 2) were aligned and root-mean-square deviations (RMSD) of atomic positions for all Cα (residues defined in the table) were determined using PyMOL.

Structure 1	Structure 2	RMSD for all Cα in Å
***Ta*PHD.*Ta*ODD** (*Ta*PHD$_{C73-Q297}$)	***Hs*PHD2.CODD** (*Hs*PHD2$_{Q184-K408}$) (PDB: 3HQR, [2])	0.54
***Ta*PHD.*Ta*ODD** (*Ta*PHD$_{C73-Q297}$)	***Hs*PHD2.NODD** (*Hs*PHD2$_{P189-Y403}$) (PDB: 5L9V, [3])	0.39
***Ta*PHD.*Ta*ODD** (*Ta*PHD$_{C73-Q297}$)	**PPHD.EF-Tu** (PPHD$_{H7-F207}$) (PDB: 4IW3, [15])	0.92
***Ta*PHD.*Ta*ODD** (*Ta*PHD$_{C73-Q297}$)	***Cr*P4H.(Ser-Pro)$_5$** (*Cr*P4H$_{W38-G250}$) (PDB: 3GZE, [16])	2.20
***Hs*PHD2.CODD** (*Hs*PHD$_{Q184-K408}$) (PDB: 3HQR, [2])	**PPHD.EF-Tu** (PPHD$_{H7-F207}$) (PDB: 4IW3, [15])	1.57

References

1 Loenarz, C. *et al.* The hypoxia-inducible transcription factor pathway regulates oxygen sensing in the simplest animal, Trichoplax adhaerens. *EMBO Reports* **12**, 63-70, doi:10.1038/embor.2010.170 (2011).

2 Chowdhury, R. *et al.* Structural basis for binding of hypoxia-inducible factor to the oxygen-sensing prolyl hydroxylases. *Structure* **17**, 981-989, doi:10.1016/j.str.2009.06.002 (2009).

3 Chowdhury, R. *et al.* Structural basis for oxygen degradation domain selectivity of the HIF prolyl hydroxylases. *Nat. Commun.* **7**, 12673, doi:10.1038/ncomms12673 (2016).

4 Rose, N. R., McDonough, M. A., King, O. N. F., Kawamura, A. & Schofield, C. J. Inhibition of 2-oxoglutarate dependent oxygenases. *Chem. Soc. Rev.* **40**, 4364-4397, doi:10.1039/C0CS00203H (2011).

5 Otwinowski, Z., Minor, W. & et al. Processing of X-ray diffraction data collected in oscillation mode. *Methods Enzymol.* **276**, 307-326 (1997).

6 McCoy, A. J. *et al.* Phaser crystallographic software. *J. Applied Crystal.* **40**, 658-674, doi:doi:10.1107/S0021889807021206 (2007).

7 Adams, P. D. *et al.* PHENIX: a comprehensive Python-based system for macromolecular structure solution. *Acta Crystallographica Section D* **66**, 213-221, doi:doi:10.1107/S0907444909052925 (2010).

8 Emsley, P. & Cowtan, K. Coot: model-building tools for molecular graphics. *Acta Cryst. D* **60**, 2126-2132, doi:10.1107/S0907444904019158 (2004).

9 Aguilar, J. A., Nilsson, M., Bodenhausen, G. & Morris, G. A. Spin echo NMR spectra without J modulation. *Chem. Commun.* **48**, 811-813, doi:10.1039/C1CC16699A (2012).

10 Flashman, E. *et al.* Kinetic rationale for selectivity toward N- and C-terminal oxygen-dependent degradation domain substrates mediated by a loop region of hypoxia-inducible factor prolyl hydroxylases. *J. Biol. Chem.* **283**, 3808-3815, doi:10.1074/jbc.M707411200 (2008).

11 Tarhonskaya, H. *et al.* Investigating the contribution of the active site environment to the slow reaction of hypoxia-inducible factor prolyl hydroxylase domain 2 with oxygen. *Biochem. J.* **463**, 363-372, doi:10.1042/BJ20140779 (2014).

12 Flashman, E. *et al.* Evidence for the slow reaction of hypoxia-inducible factor prolyl hydroxylase 2 with oxygen. *FEBS J.* **277**, 4089-4099, doi:10.1111/j.1742-4658.2010.07804.x (2010).

13 Sievers, F. *et al.* Fast, scalable generation of high-quality protein multiple sequence alignments using Clustal Omega. *Mol. Syst. Biol.* **7**, doi:10.1038/msb.2011.75 (2011).

14 Waterhouse, A. M., Procter, J. B., Martin, D. M. A., Clamp, M. & Barton, G. J. Jalview Version 2—a multiple sequence alignment editor and analysis workbench. *Bioinformatics* **25**, 1189-1191, doi:10.1093/bioinformatics/btp033 (2009).

15 Scotti, J. S. *et al.* Human oxygen sensing may have origins in prokaryotic elongation factor Tu prolyl-hydroxylation. *Proc. Natl. Acad. Sci. U.S.A.* **111**, 13331-13336, doi:10.1073/pnas.1409916111 (2014).

16 Koski, M. K. *et al.* The crystal structure of an algal prolyl 4-hydroxylase complexed with a proline-rich peptide reveals a novel buried tripeptide binding motif. *The Journal of biological chemistry* **284**, 25290-25301, doi:10.1074/jbc.M109.014050 (2009).

17 Bamford, S. *et al.* The COSMIC (Catalogue of Somatic Mutations in Cancer) database and website. *Br. J. Cancer* **91**, 355-358 (2004).

18 Percy, M. J. *et al.* A family with erythrocytosis establishes a role for prolyl hydroxylase domain protein 2 in oxygen homeostasis. *Proc. Natl. Acad. Sci. U.S.A.* **103**, 654-659, doi:10.1073/pnas.0508423103 (2006).

19 Arsenault, P. R. *et al.* A Knock-in Mouse Model of Human PHD2 Gene-associated Erythrocytosis Establishes a Haploinsufficiency Mechanism. *J. Biol. Chem.* **288**, 33571-33584, doi:10.1074/jbc.M113.482364 (2013).

20 Chowdhury, R., Hardy, A. & Schofield, C. J. The human oxygen sensing machinery and its manipulation. *Chem. Soc. Rev.* **37**, 1308-1319, doi:10.1039/b701676j (2008).

21 Epstein, A. C. *et al.* C. elegans EGL-9 and mammalian homologs define a family of dioxygenases that regulate HIF by prolyl hydroxylation. *Cell* **107**, 43-54 (2001).

22 Hirsila, M., Koivunen, P., Gunzler, V., Kivirikko, K. I. & Myllyharju, J. Characterization of the human prolyl 4-hydroxylases that modify the hypoxia-inducible factor. *J. Biol. Chem.* **278**, 30772-30780, doi:10.1074/jbc.M304982200 (2003).